On the Effect of Dissipation on Shear Instabilities in the Stable Atmospheric Boundary Layer

D. FUÀ

Istituto di Fisica dell'Atmosfera, Ple L. Sturzo 31, 00144 Roma, Italy

F. EINAUDI

School of Geophysical Sciences, Georgia Institute of Technology, Atlanta, GA 30332

(Manuscript received 6 July 1983, in final form 9 November 1983)

ABSTRACT

We are presenting the results of a stability analysis of a background wind shear in the presence of stable stratification and of height dependent coefficients of eddy viscosity and eddy thermal conduction. It is shown that the vertical gradients of the eddy coefficients substantially affect the phase velocities, growth rates and vertical structure of the gravity wave and are responsible for the appearance of some counter-gradient heat fluxes and Reynolds stresses. It is suggested that these gradients may explain the observed counter-gradient fluxes in the stable atmospheric boundary layer.

1. Introduction

The development of the MST radars in the last five years has substantially increased our ability to detect gravity wave activities in the atmosphere in general and in the troposphere in particular. Using mean and fluctuating components of the wind determined by such radars and temperature measured by nearby radiosonde ascents, VanZandt *et al.* (1979) and Klostermeyer and Rüster (1980) have successfully interpreted their data in terms of gravity waves generated by shear in the tropospheric jet stream.

The Boulder Atmospheric Observatory (BAO)'s 300 m tower in Erie, Colorado, instrumented at eight levels with three component sonic and "Gill" propeller anemometers, fast-response temperature sensors and accurate, slow-response quartz thermometers (see Kaimal and Gaynor, 1983), has similarly led to new insight into the role of gravity waves in the stably stratified atmospheric boundary layer.

Hunt *et al.* (1983) and Lu Nai-ping *et al.* (1983) have discussed several features of wave and turbulence structures observed at the BAO, pointing out the role of wavelike motions in transporting significant amounts of heat, at times in the counter-gradient direction.

Einaudi and Finnigan (1981) and Finnigan and Einaudi (1981), also using the BAO data, have presented a detailed study of a gravity wave-turbulence event. Because of the particularly monochromatic nature of the disturbance, the mean, wave and turbulent components were separated using a phase average operator. The measured period, horizontal wavelength and vertical structure were shown to be in good agreement with linear theory. The interaction between the wave and the coexisting turbulence were shown to depend critically on the phase relationship between the gradients of the periodic components of the wind and of the periodic fluctuations of the turbulent Reynolds stresses.

The interpretation of the data in all these cases requires accurate modeling. A good analytical model will have to produce good agreement for the period and the horizontal wavelength as well as for the vertical structure of the disturbance. Our ability, for example, to interpret a counter-gradient heat flux in terms of a linear gravity wave depends on our ability to represent accurately the amplitudes and relative phase of the periodic fluctuations in the vertical velocity and potential temperature.

It is the purpose of this paper to investigate the role of a height dependent eddy viscosity κ and thermal diffusivity κ_Θ on the stability of a background wind shear in the presence of stable stratification. It will be shown that the gradients in κ and κ_Θ may be important in determining the amplitude of the disturbance, its vertical structure, its period and horizontal wavelength and, to the extent that linear theory is applicable, should be included when modeling events in the atmospheric boundary layer.

In Section 2, the equations of motion are outlined and the method of solution is discussed. The numerical solutions are presented and discussed in Section 3.

2. The equations of motion for a dissipative model

The linearized equations of motion for a stratified atmosphere in the presence of a background wind and with the Coriolis terms neglected can be written as

$$\bar{\rho}\left[\frac{d\tilde{u}_i}{dt} + \tilde{u}_j \frac{\partial}{\partial x_j}\bar{u}_i\right] + \frac{\partial \tilde{p}}{\partial x_i} + \delta_{i3} g\tilde{\rho} + \frac{\partial \tilde{r}_{ij}}{\partial x_j} = 0, \quad (1)$$

$$\frac{d\tilde{\rho}}{dt} + \bar{\rho}\frac{d\tilde{u}_j}{\partial x_j} + \tilde{u}_j \frac{\partial \bar{\rho}}{\partial x_j} = 0, \quad (2)$$

$$\bar{\rho}\left[\frac{d\tilde{\Theta}}{dt} + \tilde{u}_j \frac{\partial}{\partial x_j}\bar{\Theta}\right] + \frac{\partial \tilde{e}_j}{\partial x_j} = 0, \quad (3)$$

where

$$\tilde{r}_{ij} = -\bar{\rho}\bar{\kappa}\tilde{S}_{ij}; \quad \tilde{S}_{ij} = \frac{\partial \tilde{u}_i}{\partial x_j} + \frac{\partial \tilde{u}_j}{\partial x_i}, \quad (4)$$

$$\tilde{e}_i = -\bar{\rho}\bar{\kappa}_\Theta \frac{\partial \tilde{\Theta}}{\partial x_i}, \quad (5)$$

$$\frac{d}{dt} \equiv \frac{\partial}{\partial t} + \bar{u}_j \frac{\partial}{\partial x_j}.$$

Eqs. (1), (2) and (3) are the equations of momentum, continuity and heat transport. Dependent and independent variables are all nondimensional. The spatial coordinates x_i and time t are related to the corresponding dimensional variables, labeled with an asterisk, by

$$x_i = \frac{x_i^*}{h}, \quad t = \frac{t^* V}{h}, \quad (6)$$

where V and h are the characteristic velocity and length for the system; x_3 is directed vertically upwards. Pressure p, density ρ, potential temperature Θ and velocity u_i are normalized as follows

$$p = \frac{p^*}{\bar{\rho}_g^* V^2}, \quad \rho = \frac{\rho^*}{\bar{\rho}_g^*}, \quad \Theta = \frac{\Theta^*}{\bar{\Theta}_g^*}, \quad u_i = \frac{u_i^*}{V}, \quad (7)$$

where $\bar{\rho}_g^*$ and $\bar{\Theta}_g^*$ are the values of $\bar{\rho}^*$ and $\bar{\Theta}^*$ at the ground. The overbars in (7) and in the rest of this paper refer to mean quantities while the tildes refer to fluctuating ones. The coefficient of eddy viscosity κ, thermal conductivity κ_Θ and g are given by

$$\bar{\kappa} = \frac{\bar{\kappa}^*}{Vh}, \quad \bar{\kappa}_\Theta = \frac{\bar{\kappa}_\Theta^*}{Vh}, \quad g = \frac{g^* h}{V^2}, \quad (8)$$

where g^* is the acceleration of gravity; δ_{ij} is the Kronecker delta. The functions $\tilde{r}_{ij}$ and $\tilde{e}_i$ are the fluctuating parts of the Reynolds stress and heat flux respectively. Eddy viscosity and turbulent thermal conductivity are parameterized in analogy with molecular viscosity and conduction as discussed by Fuà *et al.* (1982). We have neglected terms containing the second viscosity coefficient because it is negligible for gravity waves in the troposphere (Klostermeyer, 1980). The relation

$$\tilde{\Theta}/\bar{\Theta} - \frac{1}{\gamma}\tilde{p}/\bar{p} + \tilde{\rho}/\bar{\rho} = 0, \quad (9)$$

with γ the ratio of the specific heats at constant pressure and volume, completes the set of 6 equations in 6 unknowns.

We carry out the stability analysis of (1), (2), (3) and (9) for the case of an atmospheric background dependent on x_3 only with $\bar{u}_2 = \bar{u}_3 = 0$. For such an atmosphere, one seeks solutions of the form

$$a(x_1, x_3, t) = a(x_3)\exp[i\alpha(ct - x_1)] + \text{c.c.}, \quad (10)$$

and one can cast the equations as

$$d\Phi/dx_3 = \mathbf{A}\Phi \quad (11)$$

where Φ is the complex column vector

$$\Phi = \begin{pmatrix} \phi_1 \\ \phi_2 \\ \phi_3 \\ \phi_4 \\ \phi_5 \\ \phi_6 \end{pmatrix} = \begin{pmatrix} d\tilde{u}_1(x_3)/dx_3 \\ \tilde{u}_3(x_3) \\ d\tilde{u}_3(x_3)/dx_3 \\ \tilde{\Theta}(x_3) \\ d\tilde{\Theta}(x_3)/dx_3 \\ \tilde{p}(x_3) \end{pmatrix}, \quad (12)$$

and $\mathbf{A}$ is the complex height dependent 6×6 matrix. (Elements are defined in the Appendix.) The quantity α is the nondimensional horizontal wavenumber, assumed real, and $c = c_r + ic_i$ is the normalized frequency of oscillation, in general complex; $i = \sqrt{-1}$ is the imaginary unit. It should perhaps be mentioned that for a plane wave solution of the type given by (10), the system of equations (11) does not depend on the choice of $\bar{u}_2$. The presence of any $\bar{u}_2(x_3) \neq 0$ would only affect the second-order differential equation governing the behavior of $\tilde{u}_2$. Once the solutions of (11) are calculated, $\tilde{u}_2$ and all related fluxes can be easily computed. Thus, for example, the extension to an Ekman layer profile is straightforward.

We define the turbulent Reynolds and Prandtl numbers, Re and Pr, both constant, as

$$\text{Re} = \frac{1}{(\bar{\kappa})_{\min}}, \quad \text{Pr} = \frac{\bar{\kappa}}{\bar{\kappa}_\Theta} = \frac{(\bar{\kappa})_{\min}}{(\bar{\kappa}_\Theta)_{\min}}, \quad (13)$$

where $(\bar{\kappa})_{\min}$ and $(\bar{\kappa}_\Theta)_{\min}$ are the minimum values of the eddy diffusivity and heat conduction. Thus, $\bar{\kappa}(x_3)$ and $\bar{\kappa}_\Theta(x_3)$ will have the following expressions

$$\bar{\kappa}(x_3) = \frac{\kappa_0(x_3)}{\text{Re}}, \quad \bar{\kappa}_\Theta(x_3) = \frac{\kappa_0(x_3)}{(\text{Pr} \times \text{Re})}, \quad (14)$$

with $\kappa_0(x_3)$ larger or equal to unity. Throughout the calculations, Pr is set equal to 1.

The linear system (11) is subject to six boundary conditions. Three conditions are applied at the ground where $\tilde{u}_1$, $\tilde{u}_3$ and $\tilde{\Theta}$ are set equal to zero, correspondent to the assumption of no slip at the rigid isothermal

bottom. The remaining three are radiation conditions imposed at values of x_3 large enough for the background wind and temperature to be treated as constant; the amplitude of the three solutions associated with viscosity, thermal conduction and buoyancy carrying energy into the shear layer are set equal to zero.

System (11) is a "stiff" system since, at any given height, it involves solutions, gravity waves and two dissipative waves, with vastly different height dependence. Such systems usually require special treatment (Acton, 1970). Klostermeyer (1972, 1980) uses a multilayer approach and a Gauss-Seidel group iteration to study the propagation of gravity waves in the thermosphere and the troposphere. We use a continuous model and a code developed by Scott and Watts (1977). The code determines the eigenvalues of (11) and the corresponding eigenfunctions satisfying the appropriate boundary conditions by successive iterative integrations carried out by the method of superposition of linear independent solutions. In addition to root-finding procedures and a Runge-Kutta-Fehlberg integration scheme with global extrapolation for estimating the integration errors, the code utilizes a Gram-Schmidt reorthonormalization scheme which is applied each time a loss of independence of the solutions is detected. We have been able to calculate eigenvalues of (11) for Reynolds numbers up to 5000 and we believe that even higher values for Re could be used although the procedure becomes very time consuming.

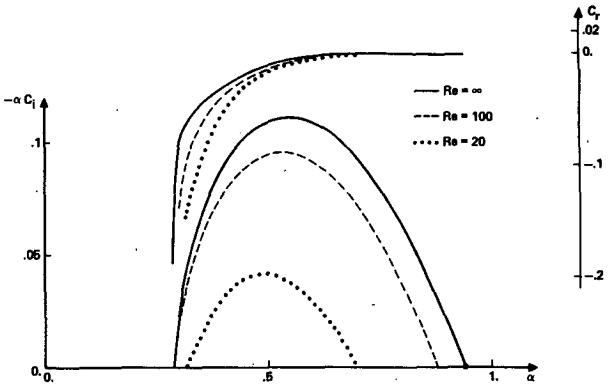

FIG. 2. Values of c_r and αc_i as a function of α for Re equal to 20, 100 and ∞ for a background defined by Model 1a: $\bar{u}_1$ as given in Fig. 1b and $\bar{T}$ is constant. The parameters used are $h/H = 0.001$, $J = 0.1$ and $\bar{T} = 280$ K.

3. Numerical results and discussion

The analysis is carried out on two background systems referred to as Model 1 and 2. Model 1 consists of an isothermal atmosphere in the presence of a background wind:

$$\bar{u}_1(x_3) = \tanh(x_3 - x_0). \tag{15}$$

We refer to this background as Model 1a when $x_0 = 5$ and Model 1b when $x_0 = 2$. The values of h/H

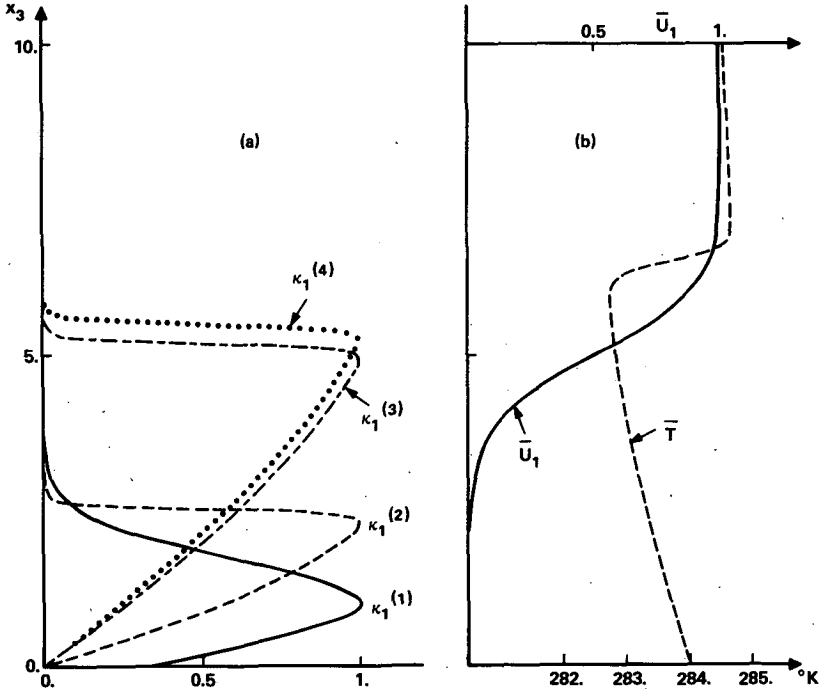

FIG. 1. (a) Profiles of the function $\kappa_1(x_3)$ defined by Eq. (16); $\kappa_1(x_3)$ is proportional to the x_3-dependent part of the eddy diffusion coefficient. (b) Background wind profile $\bar{u}_1$ and temperature $\bar{T}$ used in Model 2.

$= 0.001$, with H the scale height, and $J = n^2h^2/V^2 = 0.1$, with n^2 the Brunt-Väisälä frequency squared, are used throughout the calculations for Model 1. Model 2 is defined in terms of $\bar{u}_1$ and $\bar{T}$ plotted in Fig. 1b.

Both models are analyzed in conjunction with var-

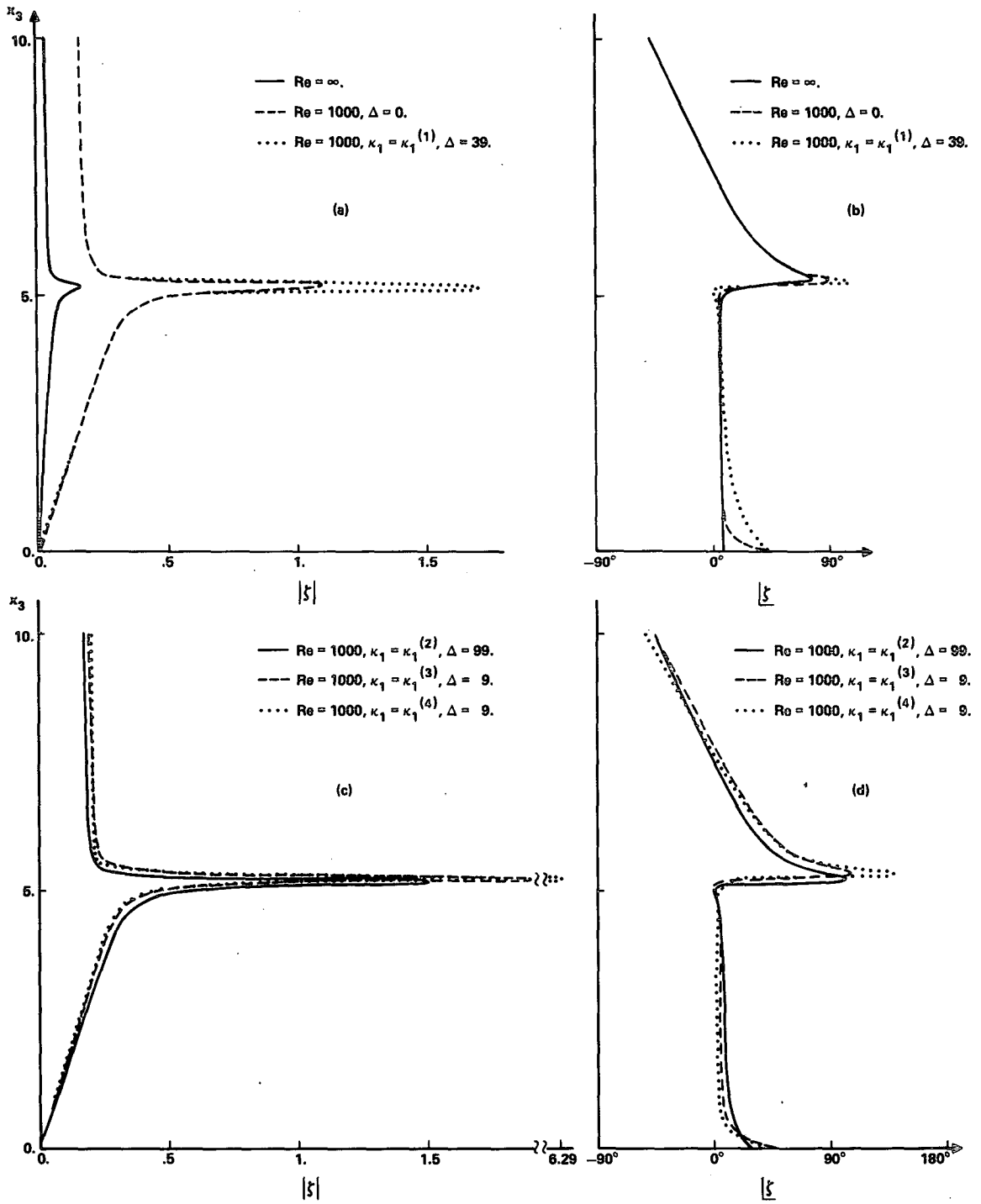

FIG. 3. Amplitudes and phases of the vertical displacements for a background defined by Model 1a. (a) and (b) describe the cases Re = ∞; Re = 1000 with Δ = 0; and Re = 1000 with $\kappa_1 = \kappa_1^{(1)}(x_3)$ and Δ = 39. The corresponding eigenvalues (c_r, $-c_i$) are (0.1816, 0.0678), (0.1853, 0.0505) and (0.1689, 0.0269) respectively. (c) and (d) describe the cases Re = 1000 with $\kappa_1 = \kappa_1^{(2)}(x_3)$ and Δ = 99; Re = 1000 with $\kappa_1 = \kappa_1^{(3)}(x_3)$ and Δ = 9; and Re = 1000 with $\kappa_1 = \kappa_1^{(4)}(x_3)$ and Δ = 9. The corresponding eigenvalues (c_r, $-c_i$) are (0.1812, 0.0302), (0.2586), 0.0344) and (0.2821, 0.0024) respectively. All phases are relative to the pressure at the ground. The amplitudes are normalized so that the nondimensional pressure at the ground is equal to 0.1.

ious profiles of $\bar{\kappa}(x_3)$ which, for convenience of presentation, are written as

$$\bar{\kappa}(x_3) = \kappa_0(x_3)\,\mathrm{Re}^{-1} = [1 + \Delta \cdot \kappa_1(x_3)]\,\mathrm{Re}^{-1}. \quad (16)$$

The profiles of $\kappa_1(x_3)$ are given in Fig. 1a. A given normalized eddy diffusivity $\bar{\kappa}(x_3)$ will be specified by the choice of $\kappa_1(x_3)$, the Reynolds number and the numerical constant Δ. These profiles are a combination

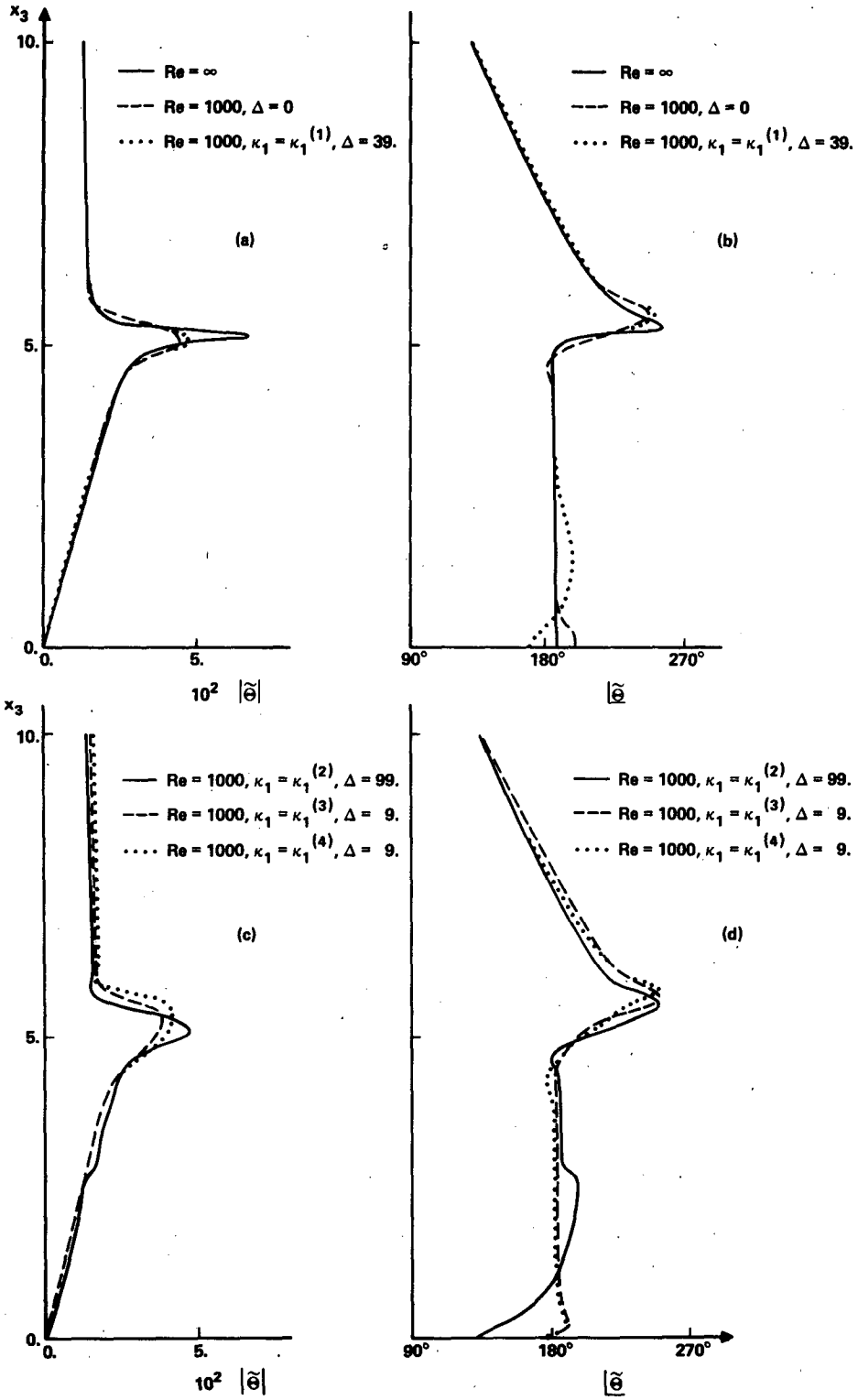

FIG. 4. As in Fig. 3 but for the amplitudes and phases of the potential temperature fluctuations $\tilde{\Theta}$.

of hyperbolic tangent and/or Gaussian functions and are in shape and magnitude quite similar to those given by Brost and Wyngaard (1978).

The cases where $\Delta = 0$ correspond to $\bar{\kappa}$ and $\bar{\kappa}_\Theta$ both constant and have been studied by Davis and Peltier (1977), where additional references may be found. They

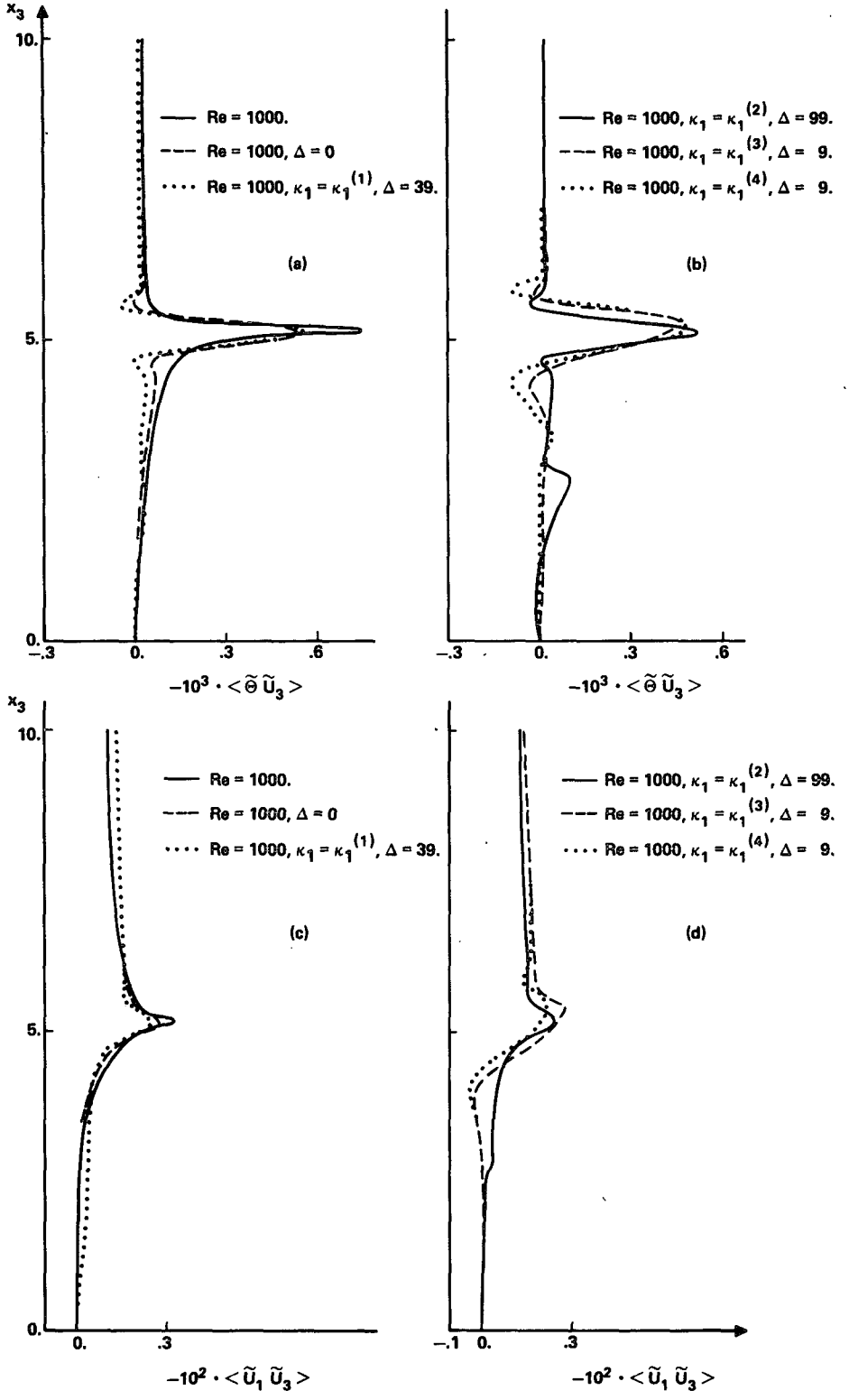

FIG. 5. Normalized heat fluxes, (a) and (b), and normalized Reynolds stresses, (c) and (d), for the cases described in Fig. 3.

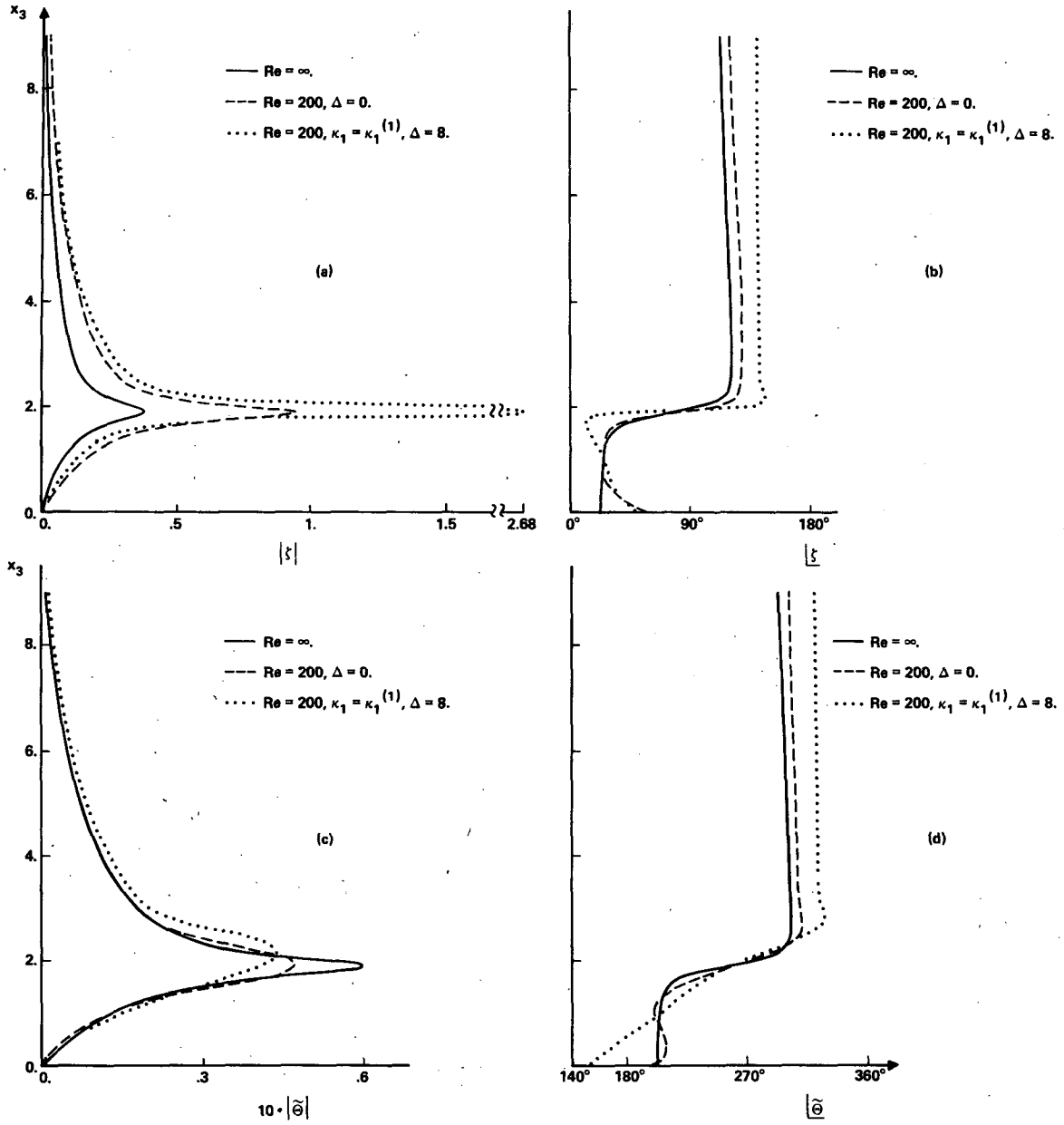

FIG. 6. (a) and (b): Amplitudes and phases of the vertical displacements for a background as in Model 1a, except that the inflection point x_0 is at 2 (Model 1b). The horizontal normalized wavenumber is now $\alpha = 0.5$. The three cases correspond to: Re = ∞; Re = 200 with $\Delta = 0$; and Re = 200 with $\kappa_1 = \kappa_1^{(1)}(x_3)$ and $\Delta = 8$. The corresponding eigenvalues $(c_r, -c_i)$ are $(-0.1197, 0.1710)$, $(-0.1245, 0.1364)$ and $(-0.0843, 0.0453)$ respectively. (c) and (d): as in (a) and (b), but for $\tilde{\Theta}$.

carry out an extensive analysis on the effect of dissipation on the domain of instability, growth rates, phase velocities and vertical structure of the waves, for a background system characterized by a hyperbolic tangent profile for both velocity and temperature with Pr = 1 and Re < 50. Their results and in particular the reduction in the growth rates appear to extend, as they suggest, to larger values of Re as indicated in Fig. 2. The smooth transition to higher values of Re is confirmed by the calculation of the eigenvalues $(c_r, -c_i)$ performed for Model 1a and $\alpha = 0.2$ as a function of Re. Here, $(c_r, -c_i)$ has the values (0.1853, 0.0505), (0.1824, 0.0582), (0.1814, 0.0625), (0.1812, 0.0634) and (0.1815, 0.0678) as Re takes the values 1000, 2000, 4000, 5000 and ∞ respectively. Similar results are obtained if, instead of the no-slip condition at the surface, we impose the free-slip condition, as was done by Davis and Peltier (1977). In this case, for Re = 1000, $(c_r, -c_i)$ is equal to (0.1905, 0.0550). In fact, none of the results presented in this paper is sensitive to this particular boundary condition.

The results in Fig. 2 and in the rest of the paper are

obtained by integrating the equations up to $x_3 = 10$, where all the background quantities are constant.

The effect of a height dependent $\bar{\kappa}$ and $\bar{\kappa}_\Theta$ is presented for three sets of calculations.

In Figs. 3–5 the results for Model 1a are presented. The wave-number is $\alpha = 0.2$ and the unstable mode is a propagating one (see Lalas and Einaudi, 1976; Davis and Peltier, 1976). Amplitudes and phases for the vertical displacement $\tilde{\zeta}$ and potential temperature fluctuations $\tilde{\Theta}$ are plotted in Figs. 3 and 4, while the normalized heat fluxes and Reynolds stresses are given in Fig. 5 for the inviscid case and various profiles of κ_1.

Similar calculations were performed for Model 1b and $\alpha = 0.5$. Here, the inflection point in the velocity profile is closer to the ground and the mode is a classical Kelvin-Helmholtz mode exponentially decaying away from the critical level, with minimal phase variation. The results for this case are summarized in Figs. 6 and 7.

Finally, the results for Model 2 which displays an elevated temperature inversion are presented in Figs. 8–10. The phase and amplitude structure indicate that this mode, with $\alpha = 0.2$, is a propagating one.

The amplitudes of the waves have all been normalized so that the nondimensional pressure at the ground is equal to 0.1. We have adopted such normalization so as to have a uniform reference level independent of the position of the critical level. In addition, pressure measurements from microbarographs are quite reliable and often have less noisy spectra than those for other variables. This point should be kept in mind in a qualitative comparison with the results of Davis and Peltier (1977) and Klostermeyer (1980).

Numerous features appear common to the cases examined:

1) The background potential temperature has positive vertical gradients, i.e., $d\bar{\Theta}/dx_3 > 0$, in all cases examined. The heat fluxes associated with the wave are counter-gradient over various height ranges as evident in Figs. 5a, b; 7a; and 10a, b. While this phenomenon is also present in the case of constant eddy diffusivity at the edges of the region about the critical level, it is clearly much more pronounced when the height dependence of $\bar{\kappa}$ is introduced. New regions where the heat fluxes are counter-gradient appear and are, in some cases, substantial. For the Kelvin-Helmholtz wave in Fig. 7a, the counter-gradient heat fluxes are entirely due to the x_3 dependence of $\bar{\kappa}$ since they are absent for Re = 200 and $\Delta = 0$ case. In most cases, a counter-gradient heat flux is present in the region close to the ground.

2) Similar countergradient Reynolds stresses are present in some of the cases analyzed, as revealed in Figs. 5d and 10d. They are clearly related to the variations in $\bar{\kappa}(x_3)$.

3) The values of $(c_r, -c_i)$ for the various cases are reported in the captions for Figs. 3, 6, and 8. The values of c_r are all within a factor of 2 from each other. The values of c_i vary over a broader range. For $\kappa_1 \neq \kappa_1^{(4)}$, the values of c_i are all within a factor of 3.7 from each other. For the case $\kappa_1 = \kappa_1^{(4)}$ in Fig. 3, $|c_i|$

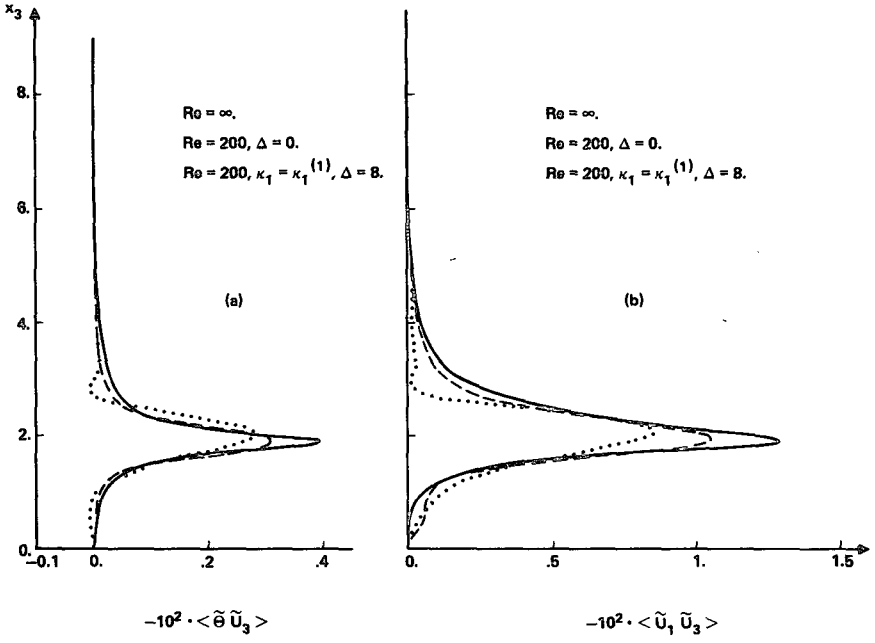

FIG. 7. Normalized heat fluxes (a) and normalized Reynolds stresses (b), for the cases described in Fig. 6.

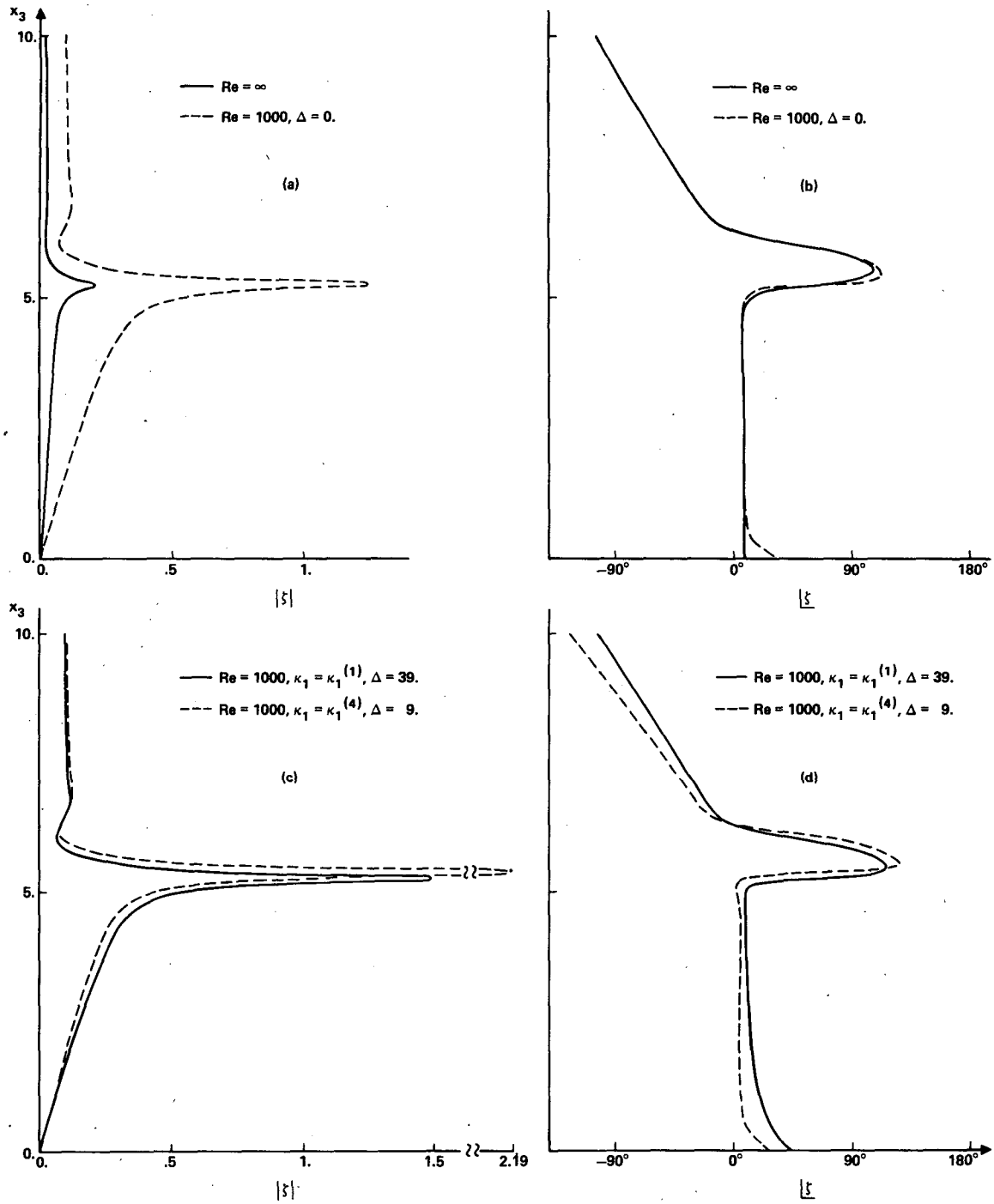

FIG. 8. Amplitudes and phases of the vertical displacements for a background defined by Model 2: $\bar{u}_1$ and $\bar{T}$ are given in Fig. 1b. The characteristic scales are $h = 40$ m and $V = 2$ m s^{-1}; $\alpha = 0.2$. (a) and (b) describe the cases Re = ∞; and Re = 1000 with $\Delta = 0$. The corresponding eigenvalues (c_r, $-c_i$) are (0.2629, 0.087) and (0.2661, 0.0741) respectively. (c) and (d) describe the cases Re = 1000 with $\kappa_1 = \kappa_1^{(1)}(x_3)$ and $\Delta = 39$; and Re = 1000 with $\kappa_1 = \kappa_1^{(4)}$ and $\Delta = 9$. The corresponding eigenvalues (c_r, $-c_i$) are (0.2593, 0.0602) and (0.3692, 0.0421) respectively.

for the inviscid case is approximately 1.3 times larger than $|c_i|$ for $\kappa_1 = 1/1000$ and 28.2 times $|c_i|$ for $\kappa_1 = \kappa_1^{(4)}$. This is clearly due to the fact that $\kappa_1^{(4)}$ extends into the region containing the critical level and strongly affects the wave growth.

4) From the graphs it is clear that the amplitude

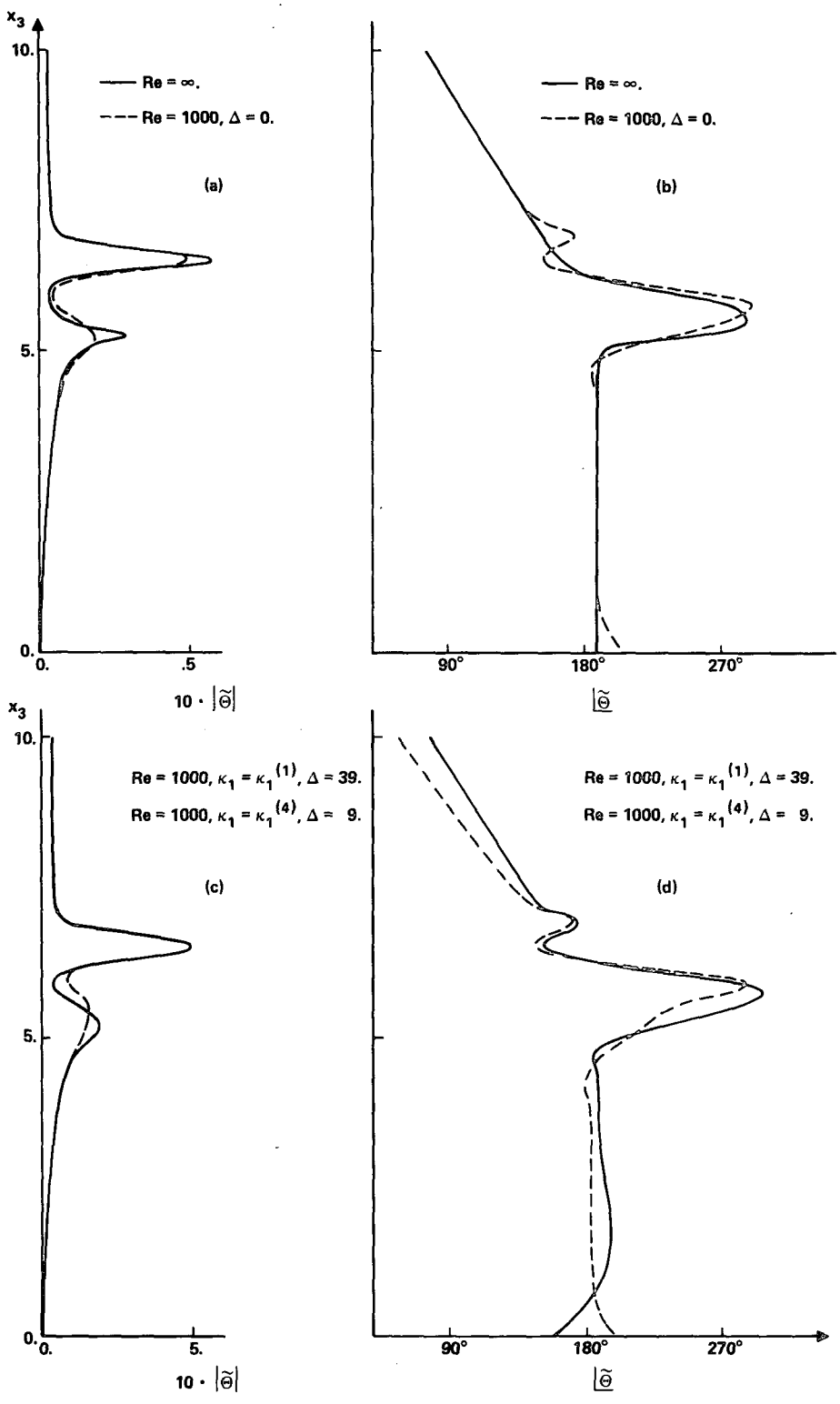

FIG. 9. As in Fig. 8 but for $\tilde{\Theta}$.

and phase of the vertical displacements and $\tilde{\Theta}$ are strongly influenced, over some height ranges, by the variations in $\bar{\kappa}$. Similar variations occur for $\tilde{u}_1$, $\tilde{u}_3$, and $\tilde{p}$, not shown here. Some of these changes can be traced to those in c_r and, more importantly, in c_i discussed above. Others are due to the local effect of the gradients

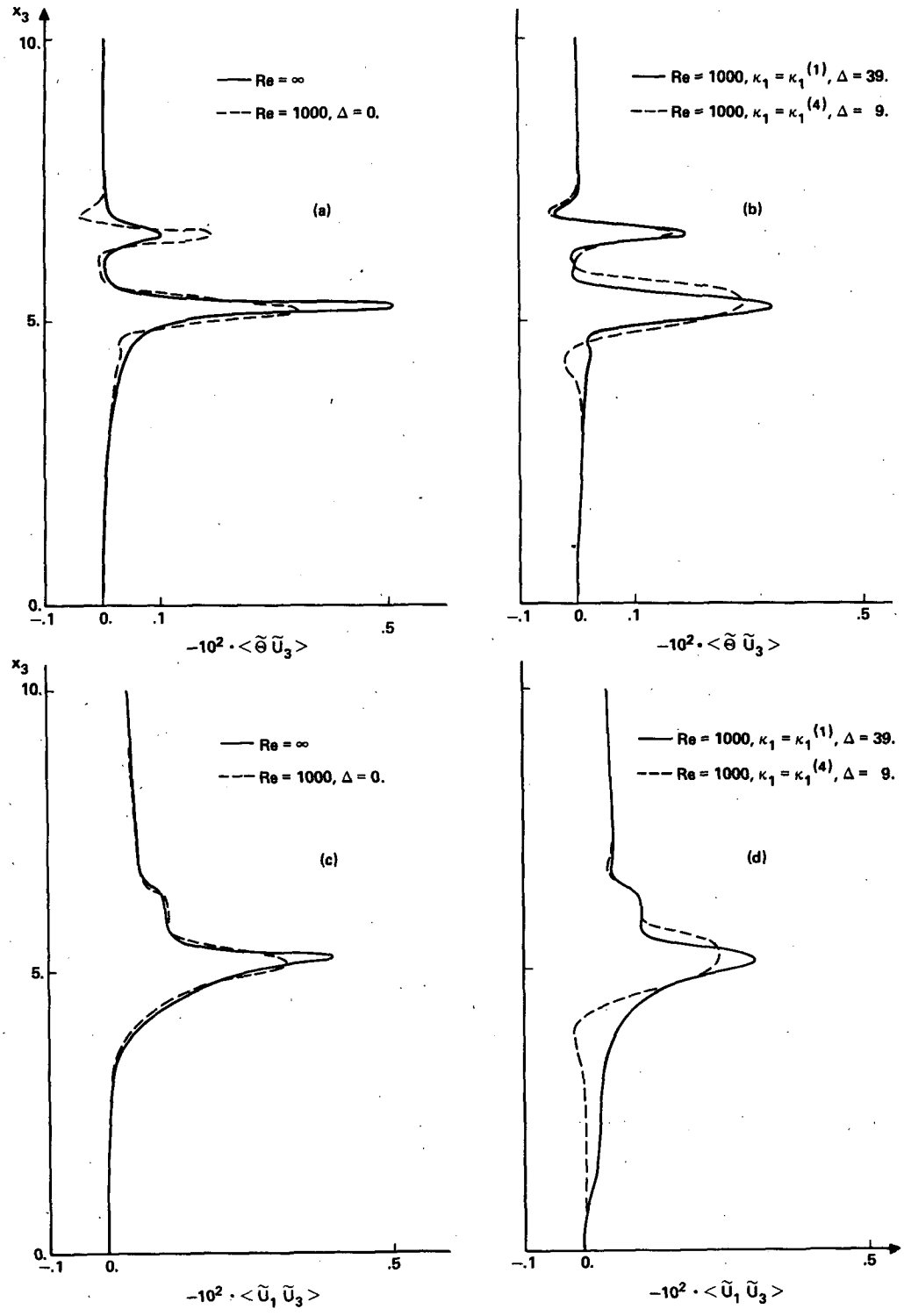

FIG. 10. Normalized heat fluxes, (a) and (b), and normalized Reynolds stresses, (c) and (d), for the cases described in Fig. 8.

of $\bar{\kappa}$. These changes in phase are indeed responsible for the appearance of counter-gradient heat fluxes and Reynolds stresses.

For Model 1, the calculations have been carried out for $h = 8.2$ m, $V = 0.48$ m s^{-1} and $T = 280$ K so that the minimum value J of the Richardson number is

APPENDIX

Elements of the Matrix A

These are the elements of the matrix **A** of Eq. (11):

$$a_{11} = \frac{-(\bar{\rho}\kappa_0)'}{\bar{\rho}\kappa_0}$$

$$a_{12} = \bar{u}'\frac{\mathrm{Re}}{\kappa_0} + \frac{i\alpha(\bar{\rho}\kappa_0)'}{\bar{\rho}\kappa_0} - i\bar{\rho}'\left(i\Omega_0\frac{\mathrm{Re}}{\kappa_0} + 2\alpha\right)\Big/\bar{\rho}$$

$$a_{13} = -i\alpha + \Omega_0\frac{\mathrm{Re}}{\kappa_0}$$

$$a_{14} = -\alpha\Omega_0\left(i\Omega_0\frac{\mathrm{Re}}{\kappa_0} + 2\alpha\right)\Big/\bar{\Theta}$$

$$a_{15} = 0$$

$$a_{16} = \mathrm{Re}\left[\Omega_0\left(i\alpha\Omega_0 + 2\alpha^2\frac{\kappa_0}{\mathrm{Re}}\right)C_0^{-2} - i\alpha\right](\bar{\rho}\kappa_0)^{-1}$$

$$a_{2i} = 0 \text{ for } i \neq 3$$

$$a_{23} = 1$$

$$a_{31} = -F\alpha\left[1 + \frac{i\alpha\Omega_0\kappa_0}{C_0^2\,\mathrm{Re}}\right]$$

$$a_{32} = -F\left[i(\bar{\rho}'/\bar{\rho})' + \alpha^2\frac{\Omega_0}{C_0^2}\left(i\Omega_0 + \alpha\frac{\kappa_0}{\mathrm{Re}}\right)\right]$$

$$a_{33} = F\left[\frac{2\alpha\Omega_0(\bar{\rho}\kappa_0)'}{\bar{\rho}C_0^2\,\mathrm{Re}} - i\frac{\bar{\rho}'}{\bar{\rho}}\right]$$

$$a_{34} = F\alpha\left[\Omega_0\frac{g_0}{C_0^2} + \bar{u}_1' + \Omega_0\frac{\bar{\Theta}'}{\bar{\Theta}}\right]\Big/\bar{\Theta}$$

$$a_{35} = -\alpha F\frac{\Omega_0}{\bar{\Theta}}$$

$$a_{36} = -\alpha F\left[\bar{u}_1' + \Omega_0 g_0\frac{(1-\gamma)}{C_0^2}\right](\bar{\rho}C_0^2)^{-1}$$

$$a_{4j} = 0 \text{ for } i \neq 5$$

$$a_{45} = 1$$

$$a_{51} = a_{53} = a_{56} = 0$$

$$a_{52} = \bar{\Theta}'\,\mathrm{Pr}\frac{\mathrm{Re}}{\kappa_0}$$

$$a_{54} = i\alpha\Omega_0\,\mathrm{Re}\frac{\mathrm{Pr}}{\kappa_0} + \alpha^2$$

$$a_{55} = -(\bar{\rho}\kappa_0)'/(\bar{\rho}\kappa_0)$$

$$a_{61} = -F\alpha\bar{\rho}\frac{\kappa_0}{\mathrm{Re}}$$

$$a_{62} = F\bar{\rho}\left[\alpha\Omega_0 - i\alpha^2\frac{\kappa_0}{\mathrm{Re}} - 2ik_0(\bar{\rho}'/\bar{\rho})'/\mathrm{Re}\right]$$

$$a_{63} = 2iF\frac{\kappa_0'\bar{\rho}}{\mathrm{Re}}$$

$$a_{64} = F\bar{\rho}[ig_0 + 2\alpha\kappa_0(\bar{u}_1' + \Omega_0\bar{\Theta}'/\bar{\Theta})/\mathrm{Re}]/\bar{\Theta}$$

$$a_{65} = -2\bar{\rho}F\alpha\kappa_0\Omega_0/(\bar{\Theta}\,\mathrm{Re})$$

$$a_{66} = -F[2\alpha\kappa_0(\bar{u}_1' + \Omega_0\gamma g_0/C_0^2)/\mathrm{Re} + ig_0]/C_0^2$$

$$F = [i - 2\alpha\Omega_0\kappa_0/(\mathrm{Re}\,C_0^2)]^{-1}$$

$$C_0^2 = \gamma R\bar{T}/V^2, \quad \Omega_0 = c - \bar{u}_1.$$

R is the gas constant and prime refers to derivative with respect to x_3.

equal to 0.1 and $h/H = 0.001$, H being the scale height. Using the value 1.25 kg m^{-3} for ρ_g^*, the coefficient of eddy diffusivity $\kappa^*(x_3)$ for Re = 1000 varies over ranges comprised between 0.07 m^2 s^{-1} and 7 m^2 s^{-1} depending on the profiles of κ_1 and the values of Δ used. The results for this model are actually applicable over a very broad range of physical situations. This follows from the fact that although the calculations are carried out for the complete set of equations, only minor variations are introduced if the Boussinesq approximation is adopted, as investigated in detail by Lalas and Einaudi (1976). It follows that essentially the same results are obtained if we set $h/H = 0$. In this approximation, the results are applicable to situations in which n^2, rather than $\bar{T}$, is set equal to the mean value in the layer of interest: the only basic parameter is the minimum of the Richardson number $J = n^2h^2/V^2$ which is set equal to 0.1 in the present calculations.

The calculations for Model 2 have been carried out with $h = 40$ m and $V = 2$ m s^{-1}. For the profiles of $\kappa_1(x_3)$ and the values of Δ used, $\kappa^*(x_3)$ varies between 0.08 m^2 s^{-1} and 3.2 m^2 s^{-1}.

The values of κ^* for both models are well within the expected values for a stably stratified boundary layer (Brost and Wyngaard, 1978; Finnigan and Einaudi, 1981).

4. Conclusions

We have presented here the stability analysis of a background wind in the presence of stratification and of height dependent coefficients of eddy viscosity and thermal diffusivity. The results show that the amplitude and phase of each gravity wave variable are affected by the vertical gradients of the eddy coefficients as are the phase velocity and the growth rate of the wave.

It follows that when a comparison is attempted between a set of experimental data with sufficient height resolution, as in the case at the BAO, and a linear model output, the actual profiles for the turbulent heat fluxes and Reynolds stresses should be included. This is a particularly critical point in the analysis of the energy budgets for the wave and the coexisting turbulence as done by Finnigan and Einaudi (1981).

The inclusion of these terms will also be essential in any attempt to study a boundary layer wave event in which the critical level is sufficiently close to the ground.

Finally, it is suggested that the counter-gradient heat fluxes often observed in the atmospheric boundary layer (Lu Nai-Ping *et al.*, 1983) may be due to gravity waves in the presence of turbulence whose intensity is dependent on height. It is understood, of course, that other mechanisms, such as nonlinear wave behavior, may produce the same effect. Gradients in the eddy coefficients are shown to be responsible for the appearance of counter-gradient Reynolds stresses in some situations.

Acknowledgments. We are grateful to Drs. D. P. Lalas and R. Richiardone for various discussions on this subject. We are also indebted to Drs. M. R. Scott and H. A. Watt for providing us with the integrating routine and several discussions on its characteristics. This work was supported in part by the NOAA Grant NA80RAD00013 and in part by NSF Grants ATM-8213784 and INT-8105101. The early stages of this work were carried out at the computing facility of the National Center for Atmospheric Research, which is sponsored by the National Science Foundation.

REFERENCES

Acton, F. S., 1970: *Numerical Methods that Work.* Harper and Row, 541 pp.

Brost, R. A., and J. C. Wyngaard, 1978: A model study of the stably stratified planetary boundary layer. *J. Atmos. Sci.*, **35,** 1427–1440.

Davis, P. A., and W. R. Peltier, 1976: Resonant parallel shear instability in the stably stratified planetary boundary layer. *J. Atmos. Sci.*, **33,** 1287–1300.

—— and ——, 1977: Effects of dissipation on parallel shear instability near the ground. *J. Atmos. Sci.*, **34,** 1868–1884.

Einaudi, F., and J. J. Finnigan, 1981: The interaction between an internal gravity wave and the planetary boundary layer. Part I: The linear analysis. *Quart. J. Roy. Meteor. Soc.*, **107,** 793–806.

Finnigan, J. J., and F. Einaudi, 1981: The interaction between an internal gravity wave and the planetary boundary layer. Part II: Effect of the wave on the turbulence structure. *Quart. J. Roy. Meteor. Soc.*, **107,** 807–832.

Fuà, D., G. Chimonas, F. Einaudi and O. Zeman, 1982: An analysis of wave-turbulence interaction. *J. Atmos. Sci.*, **39,** 2450–2463.

Hunt, J. C. R., J. C. Kaimal, J. E. Gaynor and A. Korrell, 1983: Observations of turbulence structure in stable layers at the Boulder Atmospheric Observatory. *Studies of Nocturnal Stable Layers at BAO,* Rep. 4, Jan. 1983, U.S. Department of Commerce, 129 pp. A NOAA publication available from NOAA/ERL, Boulder, CO 80303.

Kaimal, J. C., and J. E. Gaynor, 1983: The Boulder Atmospheric Observatory. *J. Climate Appl. Meteor.*, **22,** 863–880.

Klostermeyer, J., 1972: Numerical calculation of gravity wave propagation in a realistic thermosphere. *J. Atmos. Terr. Phys.*, **34,** 765–774.

——, 1980: Computation of acoustic-gravity waves, Kelvin-Helmholtz instabilities and wave-induced eddy transport in realistic atmospheric models. *J. Geophys. Res.*, **85,** 2829–2839.

—— and R. Rüster, 1980: Radar observation and model computation of a jet stream-generated Kelvin-Helmholtz instability. *J. Geophys. Res.*, **85,** 2841–2846.

Lalas, D. P., and F. Einaudi, 1976: On the characteristics of gravity waves generated by atmospheric shear layers. *J. Atmos. Sci.*, **33,** 1248–1259.

Lu Nai-ping, W. D. Neff and J. C. Kaimal, 1983: Wave and turbulence structure in a disturbed nocturnal inversion. *Bound.-Layer Meteor.*, **26,** 141–155.

Scott, M. R., and H. A. Watts, 1977: Computational solution of linear two-point boundary value problems via orthonormalization. *SIAM J. Numer. Anal.*, **14,** 40–70.

VanZandt, T. E., J. L. Green, W. L. Clark and J. R. Grant, 1979: Buoyancy waves in the troposphere: Doppler radar observations and a theoretical model. *Geophys. Res. Lett.*, **6,** 429–432.